JACS
JOURNAL OF THE AMERICAN CHEMICAL SOCIETY
Article
pubs.acs.org/JACS

Computational and Experimental Study of the Mechanism of Hydrogen Generation from Water by a Molecular Molybdenum-Oxo Electrocatalyst

Eric J. Sundstrom,[†] Xinzheng Yang,[†] V. Sara Thoi,[†] Hemamala I. Karunadasa,[†,‡] Christopher J. Chang,[†,‡,¶] Jeffrey R. Long,[†,§] and Martin Head-Gordon*[,†,‡]

[†]Department of Chemistry and [¶]Howard Hughes Medical Institute, University of California, Berkeley, California 94720, United States
[‡]Chemical Sciences Division and [§]Materials Sciences Division, Lawrence Berkeley National Laboratory, Berkeley, California 94720, United States

Supporting Information

ABSTRACT: We investigate the mechanism for the electrocatalytic generation of hydrogen from water by the molecular molybdenum-oxo complex, $[(PY5Me_2)MoO]^{2+}$ ($PY5Me_2$ = 2,6-bis(1,1-bis(2-pyridyl)ethyl)pyridine). Computational and experimental evidence suggests that the electrocatalysis consists of three distinct electrochemical reductions, which precede the onset of catalysis. Cyclic voltammetry studies indicate that the first two reductions are accompanied by protonations to afford the Mo-aqua complex, $[(PY5Me_2)Mo(OH_2)]^{+}$. Calculations support hydrogen evolution from this complex upon the third reduction, via the oxidative addition of a proton from the bound water to the metal center and finally an α-H abstraction to release hydrogen. Calculations further suggest that introducing electron-withdrawing substituents such as fluorides in the *para* positions of the pyridine rings can reduce the potential associated with the reductive steps, without substantially affecting the kinetics. After the third reduction, there are kinetic bottlenecks to the formation of the Mo-hydride and subsequent hydrogen release. Computational evidence also suggests an alternative to direct α-H abstraction as a mechanism for H_2 release which exhibits a lower barrier. The new mechanism is one in which a water acts as an intramolecular proton relay between the protons of the hydroxide and the hydride ligands. The calculated kinetics are in reasonable agreement with experimental measurements. Additionally, we propose a mechanism for the stoichiometric reaction of $[(PY5Me_2)Mo(CF_3SO_3)]^{+}$ with water to yield hydrogen and $[(PY_5Me_2)MoO]^{2+}$ along with the implications for the viability of an alternate catalytic cycle involving just two reductions to generate the active catalyst.

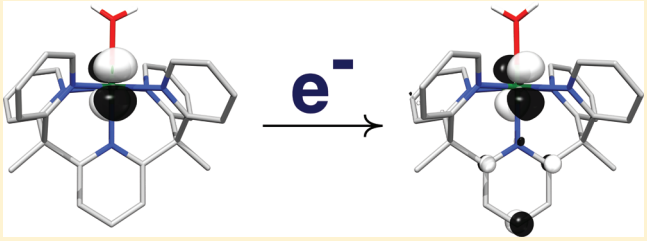

INTRODUCTION

Due to growing concerns about the impact of anthropogenic climate change, the search for carbon-neutral sources of renewable energy has become a prominent area of scientific research.[1] Solar energy capture in conjunction with a chemical energy storage system has been proposed as one potentially feasible solution to the global energy crisis.[2] One proposed strategy for chemical storage is the use of hydrogen as a fuel, because of its benign combustion byproducts, large energy density by mass (143 MJ/kg), and the potential to use H_2O to produce the fuel.[3]

In order for hydrogen to be useful as a fuel or energy storage technology, it must be produced sustainably and economically using earth-abundant, inexpensive catalysts. While naturally occurring hydrogenase enzymes containing iron and nickel cofactors are capable of significant turnover frequencies and low thermodynamic potentials,[4−8] these enzymes suffer from instabilities under industrial conditions which inhibit their deployment in a commercial setting. On the other hand, heterogeneous precious metal catalysts such as Pt exhibit high activity at low overpotentials (applied potential beyond the thermodynamic potential of the reaction) in acidic or basic media, but their high costs prohibit large-scale deployment of these systems. Consequently, significant research has been carried out on catalysts containing earth-abundant elements for the production of hydrogen. However, many of the resulting molecular H_2-evolving catalysts to date require organic solvents and additives or organic acids to reach high levels of performance.[9−15] For a comprehensive comparison of some of the latest hydrogen-evolving catalysts, see the review by Cook et al.[3]

An exciting potential candidate for a hydrogen-evolving catalyst is the molybdenum-oxo complex recently reported by Karunadasa et al.[16] Specifically the system consists of the pentadentate ligand framework 2,6-bis(1,1-bis(2-pyridyl)ethyl)-pyridine ($PY5Me_2$) supporting a molybdenum-oxo species (Figure 1). This complex shows high catalytic activity, a turnover frequency of at least 2.4 s^{-1}, and stability in pH 7 aqueous media and seawater. Since the catalyst is of molecular

Received: November 30, 2011
Published: February 22, 2012

   dx.doi.org/10.1021/ja210949r | J. Am. Chem. Soc. 2012, 134, 5233−5242

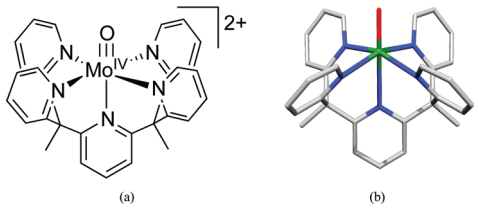

Figure 1. $[(PY5Me_2)MoO]^{2+}$: (a) shown schematically and (b) its 3D computed structure.

origin, the substantial tools of synthetic organic chemistry may be leveraged to improve upon its performance. Perhaps the most important target would be lowering the overpotential required for catalysis, which was reported as ∼−0.5 V. Experimental steps have already been taken in this direction. In particular, Sun et al.[17] showed that *para* substitution of the axial pyridine ring of $[(PY5Me_2)Co]^{+}$ lowered the catalytic potential significantly in water.

To provide both a fundamental understanding and a rational basis for synthetic modifications of $PY5Me_2$-based catalysts, it is desirable to understand the mechanism of catalysis in molecular detail and characterize the electronic structure of all intermediate species. The purpose of this paper is to present computational and experimental studies directed at this goal. In the original report, a Hg electrode was used as the working electrode due to its high overpotential for proton reduction. However, a recent report showed that the reduced Mo species forms an adsorbate on the Hg surface, thereby complicating further characterization of the active species. It was also reported that $[(PY5Me_2)MoO]^{2+}$ can catalyze the reduction of acetic acid to hydrogen in an acetonitrile solution on a glassy carbon disk electrode where the active catalyst was freely diffusing in solution.[18] Cyclic voltammetry (CV) experiments further showed that a third electron is necessary for proton reduction in both water and organic media on a glassy carbon electrode. In light of these considerations, the set of intermediates shown in Figure 2 constitutes a potentially complete description of the viable intermediates associated with catalysis, and these will be explored herein.

Within the past 20 years, electronic structure calculations have proven useful in assisting interpretation of experimental results, eliminating high-energy reaction pathways, and providing insight for rational design of synthetic changes in chemical systems. Typically, Density Functional Theory (DFT)[19−21] has been the tool of choice for the computation of redox potentials[22,23] and the modeling of catalytic processes.[24] With modern functionals, sufficient accuracy is obtained to yield useful insight into catalytic cycles without requiring prohibitive computational effort. However, electronic structure calculations, even if satisfactorily accurate, are essentially just numerical experiments, requiring other methods for analysis and chemical insight. For instance, Localized Orbital Bonding Analysis (LOBA)[25] is useful for the computational description of oxidation states and understanding the extent of electron or hole localization associated with redox changes.

Very recently, the catalytic cycle originating with $[(PY5Me_2)MoO]^{2+}$ was studied using DFT calculations by Li and Yoshizawa,[26] who showed the energetic validity of H_2 generation by reductive cleavage of water and α-H abstraction and identified a role for three reductions. The computational and experimental work reported here will validate these basic

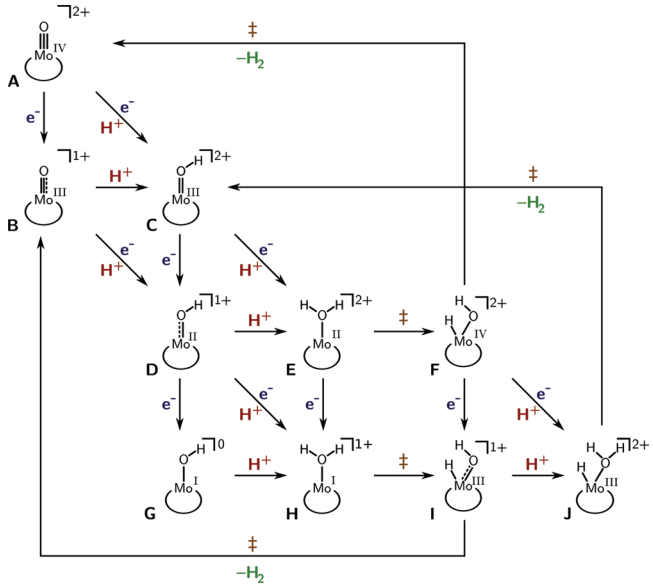

Figure 2. Cartoons of the species potentially involved in the electrocatalytic cycle of $[(PY5Me_2)MoO]^{2+}$ and their reactions. The $PY5Me_2$ ligand is represented by a circle for clarity. The symbol ‡ indicates the species are coupled through a transition structure. Metal oxidation states are those given by electron counting. The bold letters will be used to designate these species in the text.

conclusions. However, some important distinctions will also emerge. First, combining our calculations with new experiments reported here, we will conclude that the nature of the reductive steps is quite different from those reported by Li and Yoshizawa.[26] We find that the first two reductions are proton-coupled, rather than involving multiple intermediates, and the mechanism of the third reduction also differs. Second, we have found a new mechanism for the α-H abstraction step that involves a bridging water acting as a proton relay. Third, the calculated kinetics we obtain are in more satisfactory agreement with experimental values. Additionally, we extend the study of the mechanism in several distinct ways. We examine computationally in some detail the manner in which electrons are added to the complex in the three reductions. Then, on the basis of this knowledge, we perform computational experiments on the effect of chemical modifications to the $PY5Me_2$ ligand platform to explore the effect on the predicted overpotential. Finally, we also explore the stoichiometric reaction of $[(PY5Me_2)Mo]^{2+}$ with H_2O to produce $[(PY5Me_2)MoO]^{2+}$ and H_2 and its possible use as an electrocatalytic pathway.

The rest of this article is ordered as follows: We will begin by describing the computational tools used to study this system. Next, we will discuss the reductive steps of the catalytic cycle, followed by the kinetics associated with the steps occurring after the final reduction, which will include our new mechanism for H_2 formation. We will then briefly describe the stoichiometric reaction, $[(PY5Me_2)Mo]^{2+} + H_2O \rightarrow [(PY5Me_2)MoO]^{2+} + H_2$, and its possible use as an electrocatalytic reaction. Finally, we will finish by describing substituent effects and how they may be used to reduce the overpotential of the catalyst.

■ COMPUTATIONAL DETAILS

Choice of Density Functional. Three different functionals with differing treatments of exchange were explored: B3LYP,[27] BP86,[28,29]

dx.doi.org/10.1021/ja210949r | J. Am. Chem. Soc. 2012, 134, 5233−5242

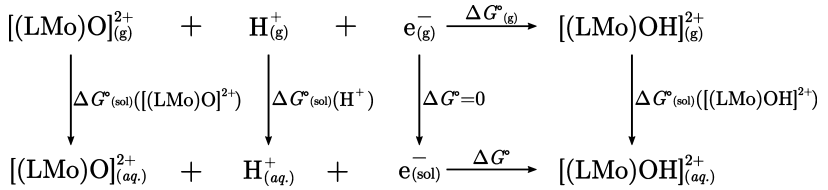

Figure 3. Thermodynamic cycle of the first reaction used to relate calculations to experimental $E_{1/2}$ values. ΔG_{sol} is the free energy of solvation. The letter L is used in place of $PY5Me_2$ for simplicity. Other reactions follow a similar pattern, with $[(LMoO)]^{2+}$ and $[(LMo)OH]^{+}$ replaced by the pertinent species and the appropriate number of protons and electrons for the reaction.

and ωB97.[30] The results necessarily depend on the choice of functional, and since different approximate functionals perform with different levels of accuracy on different problems, an appropriate choice for the systems at hand is important. The energetic results found with the BP86 functional most closely correspond to the experimental reduction potentials; indeed, the B3LYP and ωB97 functionals give the wrong sign for the first reduction. Throughout the rest of this study, we present BP86 results unless otherwise specified. The relative energies obtained with all functionals are given in the Supporting Information, Table S1. The choice of BP86 has many precedents: it has already been widely used in many successful studies of transition-metal-containing systems,[31−38] including those where hydrogen binding and release is involved.[39−41]

Quadrature Grids and Basis Sets. Exchange-correlation functionals were calculated with a larger than standard numerical quadrature grid with 70 radial points and 302 Lebedev angular points, in the interest of keeping energy, gradient, and Hessian calculations numerically consistent. Three basis sets were used in the calculations. First, a medium-sized basis including the SRSC effective core potential[42] for the Mo and cc-pVDZ[43] for all other atoms was used for the initial transition structure searches. Second, a medium-sized basis set consisting of the all-electron SV plus polarization of Ahlrichs et al.[44] for Mo and 6-31G*[45] for all other atoms (denoted SV-P/6-31G*) was used with the B3LYP functional for optimizations and frequencies. Third, a larger basis denoted as TZV-P/6-311G** was used for single-point energy calculations. It consists of the all-electron TZVP basis[44] with the original f function split into two f's and a g with contraction coefficients of 0.533380331, 1.60014099, and 1.04835114, respectively, for Mo, 6-311++G** functions for H and N, and 6-311G** functions for C and O.

Software and Algorithms. All calculations were performed in a customized version of the Q-Chem package,[46] using unrestricted orbitals. Guess densities for all calculations were produced by superposition of converged fragments of the ligand and molybdenum-oxo core.[47] Unrestricted SCF calculations were performed using the Relaxed Constraints Algorithm (RCA),[48,49] until a threshold of 10^{-3} or 10^{-5} Hartrees as necessary, followed by Geometric Direct Minimization[50] to a convergence of 10^{-9} Hartrees. For certain cases where convergence was difficult to reach, RCA alone was used to reach the 10^{-9} Hartrees target. After stationary points of the wave function were found, a stability analysis[51] was performed on all solutions to determine its nature; if a saddle point was found, a downhill step was taken and then reminimized. Frequency calculations within the harmonic approximation were used to compute gas-phase free energies, G(298.15 K). Since the lowest energy spin state for transition metal species is not obvious, at least two spin states for each species were calculated, the respective geometries were minimized, and the lowest energy spin state was then selected. Table S1 contains the absolute energies of all calculated spin states.

Localized Orbital Bonding Analysis (LOBA). LOBA[25] is employed for analyzing the oxidation state of the Mo throughout the catalytic cycle, and to assess the extent to which Mo electrons are delocalized. It is a combination of two parts: first a localization of molecular orbitals and then a subsequent orbital-by-orbital population analysis to determine metal oxidation states. The population value provides a measure of the density at a metal center for each electron and thus allows one to count the number of electrons at that center and calculate the oxidation state. The Pipek−Mezey algorithm[52] was utilized for the localization procedure. LOBA was performed using Löwdin population analyses.[53,54] All oxidation states were calculated using LOBA at the BP86/TZV-P/6-311G** level of theory.

Optimizations and Solvation. As a starting point, the solid-state structure of the dication ($[(PY5Me_2)MoO]^{2+}$) obtained from single-crystal X-ray diffraction studies was optimized so as to relax to its gas-phase geometry. This relaxation was performed so the species for which crystal structures are unavailable may be compared consistently. The subsequent species in the cycle were created by addition of hydrogen atoms and electrons, followed by relaxation to their individual gas-phase geometries. All transition structures were confirmed following the intrinsic reaction coordinates to products and reactants. While solvation is entirely neglected in the optimizations, it is manifestly critical in assessing the relative energies of intermediates that have different charges, and may also be important for the relative energies of intermediates with the same charge. However, for a hydrogen-bonding solvent like water, there are well-known limitations and ambiguities with even the most useful of polarizable continuum solvation (PCM) models.[55−57] These models disregard specific solvent−solute interactions, such as hydrogen bonds, which in our context amounts to disregarding the interactions between waters and the molybdenum-oxo or hydroxy species, which are potentially significant. Therefore, as will become clear in the Results and Discussion, we instead use experimental information to infer the change in solvation energy for species with different charges. To briefly introduce the approach taken in this study: the experimental evidence indicates the protonated species **C** exists in solution; therefore, it must have a lower free energy than that of the unprotonated species **B**. However, because of the reduction in charge, in the gas phase the energy of **B** is lower than that of **C**, and this difference needs to be made up by solvation and thus sets a lower bound on the differential solvation energies. We neglect any possible change in solvation energy for species with the same charge (including transition structures), which is partly justified by the fact that different intermediate species in the catalytic cycle have roughly the same cavity size and thus solvent reorganization energies are likely to be small.

Electrochemical Aspects. In order to compare the results of gas-phase electronic structure calculations to solution-phase electrochemical measurements, thermodynamic cycles of the form shown in Figure 3 were modeled.[58] The gas-phase calculations, including frequency calculations to account for the thermal and entropic contributions, allow for the computation of the upper portion of the cycle. The free energy for the reaction is given by eq 1.

$$\begin{aligned}\Delta G^{\circ} &= G_g([(LMo)OH]^{2+}) + \Delta G^{\circ}_{sol}([(LMo)OH]^{2+}) \\ &\quad - [G_g([(LMo)O]^{2+}) + G_{sol}([(LMo)O]^{2+}) \\ &\quad + \Delta G_{sol}(H^{+})]\end{aligned} \tag{1}$$

To relate the values calculated to experimental values obtained by CV, the reaction free energy must be shifted relative to the absolute potential of the standard electrode used in the given experiment, which is the standard hydrogen electrode (SHE). There have been many values published for the absolute potential of the SHE (98.7−102.4

dx.doi.org/10.1021/ja210949r | J. Am. Chem. Soc. 2012, 134, 5233−5242

Table 1. Averaged Values for Parameters from Two $[(PY5Me_2)MoO]^{2+}$ Molecules in the Unit Cell of $[(PY5Me_2)MoO](CF_3SO_3)_2$ (Standard Deviations in Parentheses), Compared to the Calculated Geometry of Resting State A

	bond lengths (Å)			bond angles (deg)		
	Mo−O	Mo−N_{ax}	Mo−N_{eq} (av)	N_{ax}−Mo−O	N_{ax}−Mo−N_{eq} (av)	Mo−N_{ax}−C_{ax}
exptl	1.685(3)	2.315(3)	2.159(1)	175.9(1)	81.1(4)	178.5
calcd	1.662	2.385	2.205	179.8	80.5	179.2
abs error	0.02	0.09	0.05	4.0	0.6	0.7
% error	1.4	3.0	2.2	2.2	0.8	0.4

kcal/mol).[59−62] We have chosen the value reported by Isse and Gennaro,[62] 98.72 kcal/mol, because this value was computed using the reference state for the electron (0 level for the electron energy in a vacuum at 0 K), which relates most directly to computational chemistry calculations. Another piece necessary to compute the free energy of this reaction is a sufficiently accurate reference value for the solvation free energy of the proton, $\Delta G_{sol}(H^+)$. A number of values[61−65] were considered, all of which lay in the range of −266.7 to −263.12 kcal/mol, and the value of −263.12 kcal/mol reported by Isse and Gennaro[62] was chosen for consistency with the value chosen for the shift with respect to SHE. Finally, a correction to relate the standard-state concentrations (1 M) to the experimental concentration of H^+ (10^{-7} M) must be added (see eq 2, where Q is the reaction quotient).

$$\Delta G^{\circ\prime}_{(T=298.15K)} = \Delta G^\circ + RT \ln\left(\frac{Q^{\circ\prime}}{Q^\circ}\right) \quad (2)$$

$$= \Delta G^\circ + RT \ln\left(\frac{\dfrac{1\text{ M}[(LMo)OH]^{2+}}{1\text{ M}[(LMo)O]^{2+}\cdot 10^{-7}\text{ M}H^+}}{\dfrac{1\text{ M}[(LMo)OH]^{2+}}{1\text{ M}[(LMo)O]^{2+}\cdot 1\text{ M}H^+}}\right)$$

$$= \Delta G^\circ + 9.55\text{ kcal/mol} \quad (3)$$

Recently, Solis and Hammes-Schiffer[66] have employed isodesmic reactions to compute reduction potentials and pK_a's of cobaloximes participating in hydrogen evolution reactions. This approach is quite powerful since it accounts for the systematic computational error in DFT due to approximate functionals and basis set incompleteness. However, in order to be exploited fully, it is beneficial to have reference reduction potentials for reactions which are of a similar nature (i.e., oxidation state and ligand species) to those being studied. Reference reactions similar to the ones studied in this paper are difficult to obtain due to the rarity of high molybdenum oxidation states and recent development of the ligand. Therefore, isodesmic reactions were not utilized in this study.

RESULTS AND DISCUSSION

Reductions. In order to be able to realistically model the catalytic cycle of $[(PY5Me_2)MoO]^{2+}$, we first need to prove that we are able to obtain accurate geometric structures for these species. The geometry of the resting state, **A** in Figure 2, was reproduced to serve as a benchmark for the geometry optimization of the subsequent species in the catalytic cycle. Table 1 shows that the calculated structure is in reasonable agreement with the crystal structure; for an image of the crystal structures see Supporting Information Figure S1, and for images of the calculated structures see Figure S3. The same level of theory was then used to compute the geometries for the rest of the species in Figure 2.

The first fork in the reaction pathway occurs at **A**→**C** or **A**→**B** in Figure 2. Because the electronic structure calculation favors the reduction of net positive charge, the gas-phase energy of **B** is much lower than that of **C** . Therefore, in order to distinguish between these two pathways, the pH dependence of the first reduction of $[(PY5Me_2)MoO]^{2+}$ over a pH range of 4.1−7.7 was studied at a glassy carbon electrode using CV, as shown in Figure 4. The plot of the peak potential, E_p, of the first reduction versus pH shows a linear fit with a slope of 44 mV. If this was a reversible single-proton-coupled-to-electron event, we would expect a slope of 59 mV; however, the deviation in our value may be a result of the irreversibility of the first redox event. Thus, the experimental evidence indicates that the first reduction involves a protonation, favoring **C** as the chemically relevant species. In order to make the experimental and theoretical results consistent, it is necessary to consider the solvation energy of the **B** and **C** species, because the more highly charged species, **C**, will be favored in aqueous media. Using the experimental result (G_{aq}(**C**) < G_{aq}(**B**)) as a guide, we find a lower bound on the solvation free energy difference,

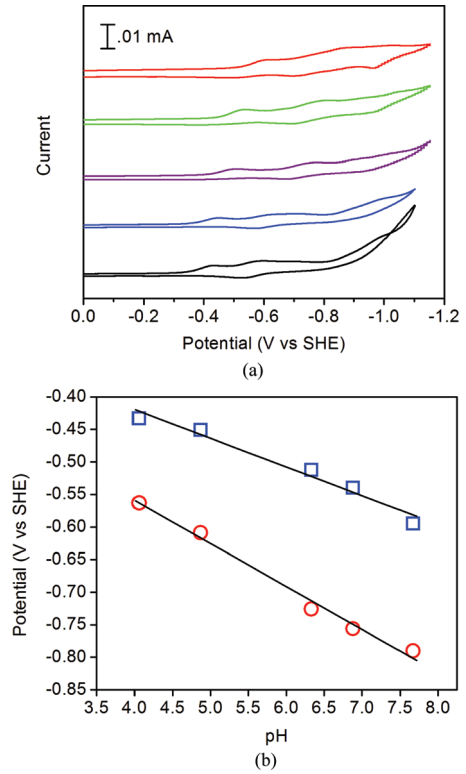

Figure 4. (a) Cyclic voltammogram of $[(PY5Me_2)MoO]^{2+}$ (**A**) in 1.0 M buffered aqueous solutions at pH 7.7 (red), 6.9 (green), 6.3 (magenta), 4.9 (blue), and 4.1 (black) on a glassy carbon disk electrode. (b) Plot of the first and second reduction potentials versus pH. Blue squares are the peak potentials of the first reduction, E_p, with a linear least-squares fitted slope of 44 mV in black, and red circles are the $E_{1/2}$ of the second reduction, with a linear least-squares fitted slope of 66 mV. Both these slopes are comparable to 59 mV, which is indicative of a proton-coupled electron-transfer event. For the experimental details, see the Supporting Information.

dx.doi.org/10.1021/ja210949r | J. Am. Chem. Soc. 2012, 134, 5233−5242

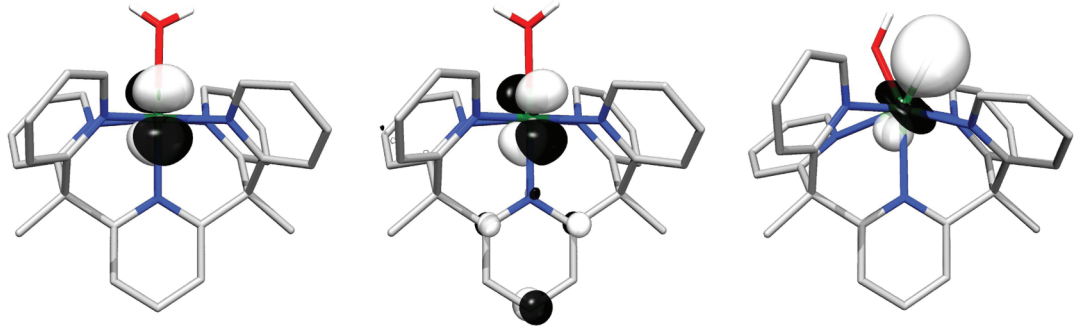

(a) **E** (b) **H** (c) **I**

Figure 5. Isosurface (0.07 au) plots of a representative localized orbital of **E** and one of the orbitals of **H**, which by contrast shows substantial delocalization to the pyridine rings. This indicates that functionalization of the pyridine rings may result in changes in the relative energetics and consequently the overpotential. The delocalization in **H** is in contrast to **I**, where the only metal electrons that exhibit delocalization are now forming the Mo−H bond with a bond length of 1.7 Å .

ΔG°_{sol} (**C**) − ΔG°_{sol} (**B**), of 3.7 eV. The computed reduction potential of **A**→**C** is 0.48 V, which compared to experiment, E_p = 0.55 V, is quite satisfactory.

Now that the calculated result is consistent with the experiment, the electronic structures of species **B** and **C** may be examined in more detail. By comparing the LOBA result of **B** to that of **A** (Figure S2), we are able to say that the additional electron has been added to an orbital of antibonding character, which reduces the bond order of the Mo−O bond. (Based on the LOBA analysis, it changes from 3 to 2.5.) This weakening of the bond makes the oxo ligand more nucleophilic, which in turn increases its pK_a, explaining why **C** is the more thermodynamically stable species. The electronic structure of species **C** is what one would expect for a molybdenum-hydroxy species with a LOBA-calculated oxidation state of 3+.

For a second reduction starting from **C**, the possible pathways are either direct reduction, **C**→**D**, or a proton-coupled reduction, **C**→**E**. CV experiments were again employed with computation to distinguish between these pathways. Experimentally, the second reduction process is quasi-reversible, with a well-defined $E_{1/2}$. When the $E_{1/2}$ is plotted against pH, a linear fit with a slope of 66 mV was obtained, suggesting a second one-proton, one-electron coupled process (Figure 4). The same logic concerning solvation effects may be applied, resulting in a lower bound on the solvation energy difference favoring **E** over **D** by 4.0 eV. This becomes our sharpened estimate of the differential solvation of the 2+ and 1+ species, and this value was added to the free energies of **B**, **D**, **H**, and **I** to define the relative energetics. The computed reduction potential of this step is then 0.47 V, which is ∼0.3 V under the experimental $E_{1/2}$ of 0.76 V. This larger difference may be due to our assumption that the solvation free energies of **A** and **C** are exactly the same. Another source of computational error comes from the intrinsic errors associated with the density functional.[22] In addition, these errors may be due to omission of the electrode surface in the modeling.

The next step of the cycle involves either hydride migration, **E**$\overset{\ddagger}{\rightarrow}$**F**, or the third reduction, **E**→**H**. When the free energies of these species are compared, including the solvation correction discussed above, the energy of **H** is almost equal to that of **F**, but the pathway to **F** is impeded by slow kinetics, which will be discussed later. Furthermore, it is known from experiments that the electrocatalysis contains three reductions, and thus even if **E**$\overset{\ddagger}{\rightarrow}$**F** were to occur, it would be further reduced to **I**, where it will rejoin the other pathway. The computed potential for the reduction of **E**→**H** is 0.77 V; this is to be compared to the experimental onset potential of the catalytic wave ∼1.1 V vs SHE at a glassy carbon electrode. Our potential is under this experimental value by ∼0.3 V, similar to the deviation for the second reduction, for the same possible reasons listed above. The minimum potential required for $[(PY5Me_2)MoO]^{2+}$ to be employed electrocatalytically is the same as is required to produce species **H**, and thus this potential should be most directly related to the overpotential for the catalyst.

Based on the LOBA analysis, the electronic character of **H** differs from that of **E** by much more than the addition of an extra electron to Mo. The localized orbitals that are primarily on molybdenum have much lower populations for species **H** than those found in **E** (Table S2), indicating the molybdenum electrons in **H** are partially delocalized. This delocalization can also be seen visually in the localized molecular orbitals shown in Figure 5, where panel (a) for **E** is well-localized, while panel (b) for **H** exhibits clear delocalization onto the axial pyridine group. An electron-donating group may be able to stabilize these partially delocalized orbitals, which is significant since the stability of **H** connects to the overpotential of the catalyst. We shall return to this topic in the subsection on Substituent Effects.

Following the formation of **H**, either intramolecular hydride transfer to **I** or proton addition to **J** could give the next intermediate in the cycle. We eliminate **J** as it is substantially higher in energy (0.5 eV) than **I**, despite inclusion of the solvation correction. **I** is connected to **H** by a transition structure which is discussed in the next section, on Kinetics; here, we shall focus on the electronic structure of the thermodynamically stable **I** . The LOBA-calculated oxidation state of **I** is 3+, which agrees with standard electron counting. The d-orbitals on the molybdenum center no longer show the significant delocalization that they did in species **H**, apart from two electrons that yield the metal−hydride bond, as shown in panel (c) of Figure 5.

Kinetics. The chemical transformations associated with intramolecular hydride transfer, **H**→**I**, and subsequent H_2 release are likely to have significant barriers, and therefore exert kinetic control on the overall turnover rate of the catalyst.

dx.doi.org/10.1021/ja210949r | J. Am. Chem. Soc. 2012, 134, 5233−5242

We shall investigate the kinetics of proton reduction under the assumption that the electron-transfer steps are not rate limiting. Two transition structures for the evolution of hydrogen by $[(PY5Me_2)MoO]^{2+}$ were found: one for the transformation from **H** to **I** and the second from **I** to the release of hydrogen gas shown in Figure 6 and summarized energetically in Figure 7. Using the standard formulation of transition state theory (TST)[67,68] (eq 4), the rates in Table 2 were calculated. For the

$$k_{TST} = \frac{k_B T}{h} e^{-\Delta G^{\ddagger}/RT} \quad (4)$$

overall rate, a steady-state approximation ($dI/dt = 0$) was made, and the total rate was calculated using $\Delta G^{\ddagger} = G(\mathbf{H}\overset{\ddagger}{\rightarrow}\mathbf{I}) - G(H)$. Some comparison against experimentally measured kinetics is possible, though caution is necessary. We emphasize that the experimental rate is the lower limit for the catalytic rate[16] which was obtained under an applied overpotential. Nevertheless, to roughly assess the calculated barriers, the experimental rate of 2.4 $mol_{H_2}/mol_{catalyst}$·s has been back-converted to $\Delta G^{\ddagger}$ using the inverse of eq 4, resulting in a value of ~17 kcal/mol; it should also be noted that because only one temperature measurement was taken, there are large uncertainties associated with this computed $\Delta G^{\ddagger}$.

As a hydrogen-bonding solvent, water can play an explicit role in stabilizing transition structures. We investigated this effect by including a water near **I** (Figure 8), but instead found a completely new transition structure for the release of hydrogen. The water molecule acts as a bridge between the two hydrogens of **I**, reducing the distance between the reacting hydrogens by 0.2 Å, which in the original computed structure were quite distant, 1.98 Å. In the transition structure the water acts a proton relay, losing one of its hydrogens to form H_2 while simultaneously abstracting the hydrogen from the hydroxy species to regenerate itself. The energetics for this new mechanism are shown in Figure 9, and the rate and barrier are shown in Table 2. The barrier for this new mechanism is ~3 kcal/mol lower in energy, and the rate is accordingly much higher (2.62 s^{-1}) for this step of the reaction. p This decrease in the reaction barrier indicates that it is important, if not essential, to consider explicit interactions between a solvent molecule and the reaction center, especially when the solvent may catalyze the reaction due to its molecular composition. Using this new transition structure to compute the overall rate (still assuming a steady-state of **I**) we obtain a a barrier of 25.1 kcal/mol. This barrier is only 8 kcal/mol larger than that of the calculated experimental one. This is likely to be within the errors associated with our calculations (approximate functionals, simple solvation treatment, and neglect of tunneling) and the error in determining the experimental barrier.

Stoichiometric Reaction. As previously reported,[16] the stoichiometric reaction between $[(PY5Me_2)Mo(CF_3SO_3)]^+$ and water leads to the formation of $[(PY5Me_2)MoO]^{2+}$ and evolution of H_2. Hydrogen production was confirmed by mass spectrometry, and the oxo was shown to originate from water by observing the isotopic shift in the infrared spectrum of the Mo═O bond upon reaction in $H_2{}^{18}O$. If the triflate is labile and exchanges with a water, the species initially formed is $[(PY5Me_2)Mo(OH_2)]^{2+}$ (**E**), and the subsequent loss of H_2 may be analyzed using the same computational tools employed for the catalytic cycle above. The experimental lability of triflate was confirmed when a crystal structure obtained upon crystallization from a solution of $[(PY5Me_2)Mo(CF_3SO_3)]^+$

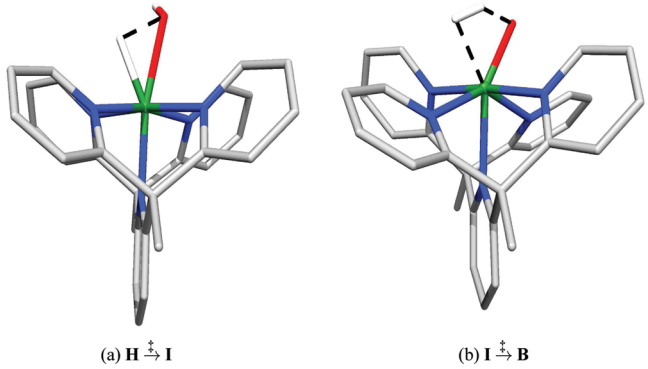

(a) $\mathbf{H} \overset{\ddagger}{\rightarrow} \mathbf{I}$ (b) $\mathbf{I} \overset{\ddagger}{\rightarrow} \mathbf{B}$

Figure 6. Geometries of transition states for (a) the transformation to a metal hydride and (b) the direct release of H_2. The bonds being broken are shown as dashed lines.

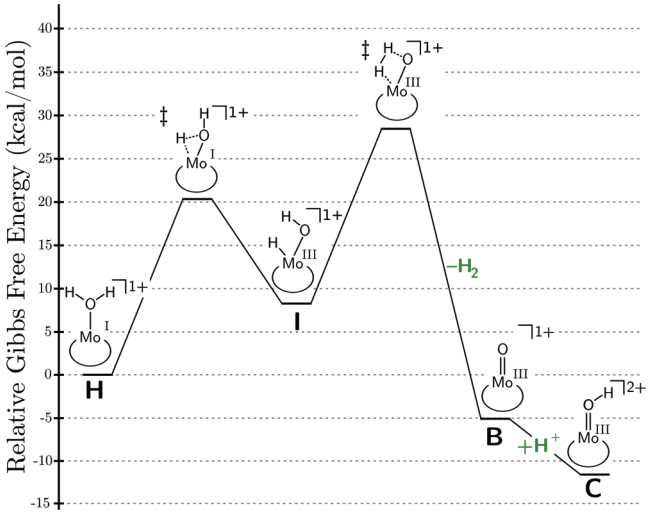

Figure 7. Gibbs free energy diagram for the liberation of hydrogen from **H** and the re-formation of **B**. The release of H_2 is exergonic by 5.0 kcal/mol and the total reaction by 11.5 kcal/mol. All species are treated with the solvation correction from the text, which is constant for all species with the same net charge.

Table 2. Rates from TST, Using Barriers Calculated at the BP86/TZV-P/6-311G Level of Theory Using the Assumptions Described in the Text, versus Experimental Values**

	$\mathbf{H}\overset{\ddagger}{\rightarrow}\mathbf{I}$	$\mathbf{I}\overset{\ddagger}{\rightarrow}\mathbf{B} + H_2$	$\mathbf{I} + H_2O \overset{\ddagger}{\rightarrow} H_2$	overall	overall + H_2O	exptl[a]
$\Delta G^{\ddagger}$ (kcal/mol)	20.3	20.1	16.9	28.4	25.1	16.9
k_{TST} (s^{-1})	8.22×10^{-3}	9.86×10^{-3}	2.62	9.21×10^{-9}	2.44×10^{-6}	2.4

[a]It should be noted that the experimental rate is for the overall reaction, and this value is a lower limit because it was obtained under an applied overpotential.

dx.doi.org/10.1021/ja210949r | J. Am. Chem. Soc. 2012, 134, 5233–5242

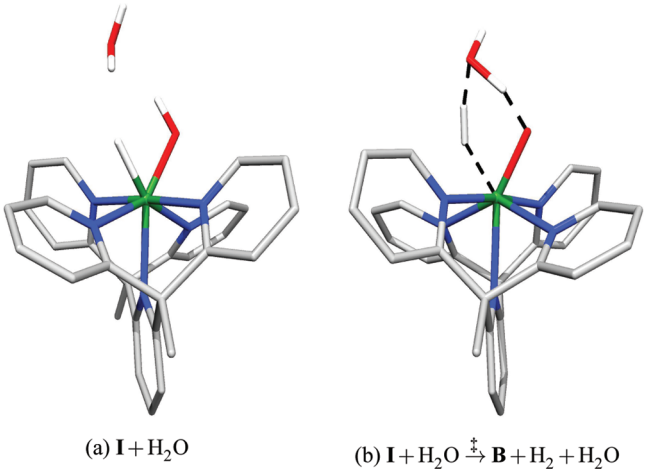

Figure 8. Geometries of (a) **I** in the presence of a water molecule and (b) the transition state for the release of H_2 including the bridging water. The bonds being broken are shown as dashed lines.

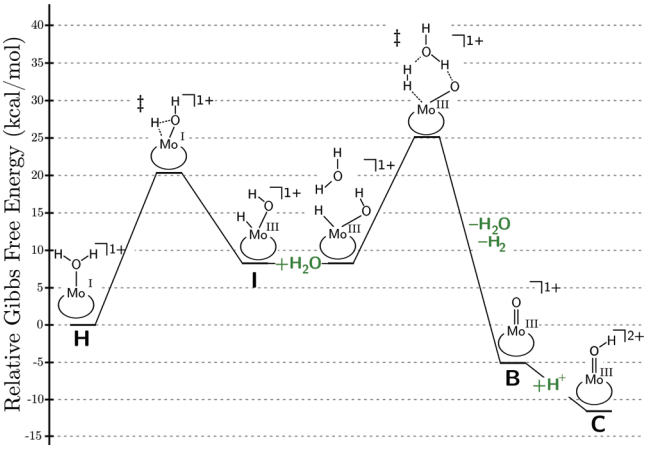

Figure 9. Gibbs free energy diagram for the liberation of hydrogen from **H** and the re-formation of **B**. The release of H_2 is exergonic by 5.0 kcal/mol and the total reaction by 11.5 kcal/mol. All species are treated with the solvation correction from the text, which is constant for all species with the same net charge. Rather than spuriously attempt to take into account the complications involved in calculating the water association energies for a molecule already solvated in water, the complexation energy was set to 0.

in acetonitrile showed substitution by a solvent molecule, as shown in Figure S4.

Accordingly, we have found transition structures for the intramolecular hydride migration, **E**→**F**, and for the subsequent evolution of H_2, yielding **A**. The structures are qualitatively similar to those discussed previously, as can be seen by comparing Figure 10 with Figure 6. The energetics of these reaction are shown in Figure 11. Using eq 4 to calculate the rate of reaction for these transition structures leads to the rates shown in Table 3. Again, for the overall rate, a steady-state approximation ($dF/dt = 0$) was made, and the total rate was calculated using $\Delta G^{\ddagger} = G(\mathbf{F}\overset{\ddagger}{\rightarrow}\mathbf{A}) - G(\mathbf{E})$. Note that a spin crossover occurs in this reaction, since the transition structure $\mathbf{F}\overset{\ddagger}{\rightarrow}\mathbf{A} + H_2$ is a singlet, whereas the **F** itself is a triplet. This spin crossover could also lower the overall rate of this reaction, though this need not be the case.[69] Finally, it is also possible that water-assisted transition structures exist, as was shown in the previous section.

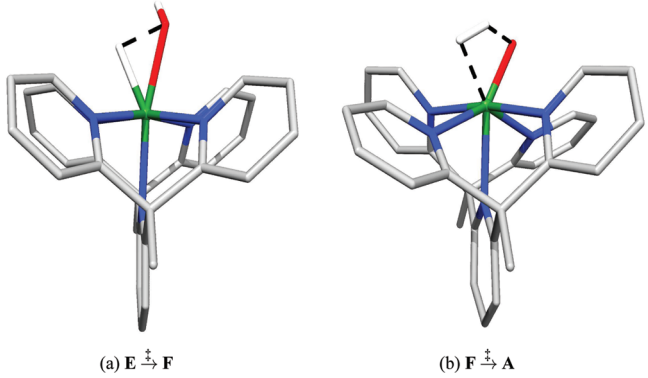

Figure 10. Geometries of transition structure involved in the stoichiometric reaction,

$$[(PY5Me_2)Mo(CF_3SO_3)]^+ \xrightarrow[-CF_3SO_3^-]{+H_2O} [(PY5Me_2)MoO]^{2+}$$

(a) Conversion to a metal hydride and (b) release of H_2.

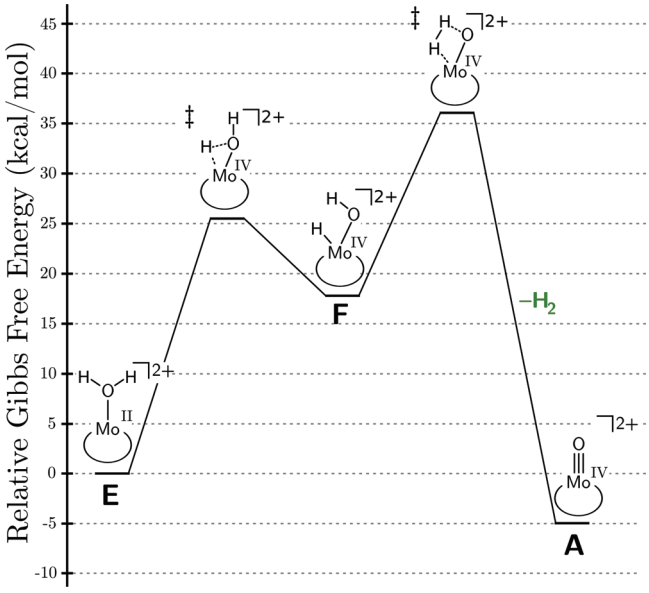

Figure 11. Gibbs free energy diagram for the liberation of hydrogen from **E**. The release of H_2 is exergonic by 4.9 kcal/mol. All species are treated with the solvation correction from the text, which is constant for all species with the same net charge.

Table 3. Rates from TST for the Stoichiometric Reaction at the BP86/TZV-P/6-311G Level of Theory**

	$\mathbf{E}\overset{\ddagger}{\rightarrow}\mathbf{F}$	$\mathbf{F}\overset{\ddagger}{\rightarrow}\mathbf{A} + H_2$	overall
$\Delta G^{\ddagger}$ (kcal/mol)	25.5	18.2	36.0
k_{TST} (s^{-1})	1.4×10^{-6}	0.27	2.41×10^{-14}

Regardless, the calculated rates of $\mathbf{E}\overset{\ddagger}{\rightarrow}\mathbf{F}\overset{\ddagger}{\rightarrow}\mathbf{A} + H_2$ are very interesting when compared to the rates of $\mathbf{H}\overset{\ddagger}{\rightarrow}\mathbf{I}\overset{\ddagger}{\rightarrow}\mathbf{B} + H_2$, the species believed to participate in electrocatalysis. This comparison explains why the third electron is necessary for electrocatalysis, despite the reduction of hydrogen being a two-electron process. The slowest rate of the 1+ species is ~4

dx.doi.org/10.1021/ja210949r | J. Am. Chem. Soc. 2012, 134, 5233–5242

orders of magnitude larger than that of the 2+ species (8.2×10^{-3} vs 1.4×10^{-6} s^{-1}, respectively). Thus, on the time scale of a CV experiment (>20 s), the species **F** is unable to form in any significant amount, and the system is only a functioning catalyst after a third reduction.

However, the stoichiometric reaction opens up an interesting possibility. If the rate of this reaction could be increased to be comparable to that of $\mathbf{H}^{\ddagger}\rightarrow\mathbf{B} + H_2$, it may be possible to bypass the third reduction, which should significantly lower the overpotential of the catalyst. The proposed cycle for this reaction is shown in Figure 12. Of course, such modifications may be synthetically challenging, or not be possible without undermining some of the positive properties of the existing catalyst. However, it certainly indicates the potential for further explorations of this catalyst architecture.

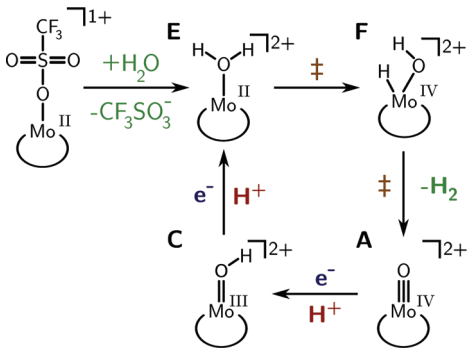

Figure 12. Proposed two-electron cycle for $[(PY5Me_2)MoO]^{2+}$, which utilizes the same mechanism as the stoichiometric reaction.

Substituent Effects. Let us briefly summarize the implications of the Reductions subsection for tuning the catalyst. The third reduction leads to intermediate **H**, and the relative energy of this species versus the prior intermediate, **E**, formally controls the overall potential bias needed for catalysis. Stabilizing **H** by ligand substitutions therefore is a path to reducing the overpotential associated with catalysis (though overpotential is also influenced by other factors as well). Comparative LOBA analysis of **H** and **E** suggests that such an effect is possible because Mo electrons in **H** exhibit delocalization onto the ligand that is not present in **E** (see Figure 5). Therefore, **H** may be stabilized and the overpotential reduced by adding electron-withdrawing groups on the *para* positions of the $PY5Me_2$ ligand platform.

In order to explore this possibility computationally, electron-withdrawing (fluorine) and electron-donating (methyl) groups were substituted at the *para* positions of all the pyridine rings (Figure 13), which are in principle synthetically feasible sites for

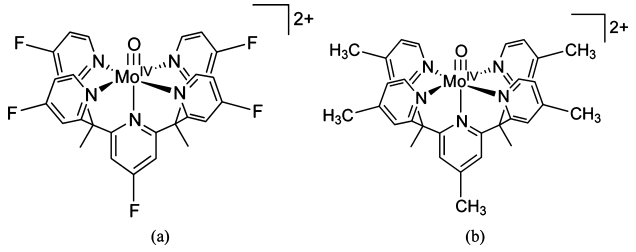

Figure 13. Schematics of the (a) fluorine- and (b) methyl-substituted species of **A**.

modification. These groups were added at the bond lengths and angles equivalent to those found by performing an optimization (B3LYP/6-31G*) on just a single substituted pyridine ring; the rest of the structure remained the same as the unsubstituted catalyst. Single-point calculations were then performed at the BP86/TZV-P/6-311G** level of theory. We assumed that the solvation corrections were unaffected by the substitutions. The shifts in reduction potentials and reaction barriers were then evaluated by isodesmic cycles, which should lead to favorable error cancellation.

First, let us summarize the calculations of substituent effects on the reduction potentials. For the first reduction, there is no change: the relative energy of **A** and **C** shifted by only 0.01 V for both substitutions. Chemically, we expect the change to be small because the relatively localized d-electrons of both **A** and **C** should be unaffected by these distant substitutions. For the second reduction, the relative energy between **C** and **E** increased by 0.04 V for the fluorination and 0.10 V for the methyl substitution. Once again these small shifts can be explained by LOBA: any electron delocalization of **E** is minor in comparison to that of species **H**. For the targeted third reduction, substituent effects stabilized **H** relative to **E** by 0.20 V for the fluorinated complex, while they led to a destabilization of 0.40 V for the methylated complex. These results demonstrate the utility of the LOBA analysis, and provide encouragement for further experimental studies.

However, it is possible that chemical substitutions in the ligand support will have implications for the kinetics of the resulting catalyst. In order to assess if the rate of the reaction is affected by the substitutions, we applied the same fluorination and methylation modifications to the transition structures for intracomplex hydride migration and H_2 elimination.

These results are interesting in that both the fluorination and methylation slightly stabilize $\mathbf{H}^{\ddagger}\rightarrow\mathbf{I}$, **I**, and $\mathbf{I}^{\ddagger}\rightarrow\mathbf{B} + H_2$ relative to **H** by ~0.1 V, as shown in Figure 14. In contrast, the two substitutions had opposite effects on the stability of **H** relative to the less reduced species. The stabilization reduces the barrier for the first rearrangement and thus increases the rate for the first step. The barrier for the α-H abstraction step was unaffected by the substitutions and is still lower than that for H_2O cleavage, which implies that the cleavage step is still rate-limiting. Therefore, reduction of this barrier by these substitutions increases the overall rate. Finally, referring back to the possibility of a two-electron redox cycle, our fluorination/methylation substitutions did not lower the rate for conversion from $\mathbf{E}^{\ddagger}\rightarrow\mathbf{F}$ enough to make it a viable pathway, and this remains an interesting challenge for future studies. A recent report by Solis and Hammes-Schiffer[70] showed for a wide variety of substituted cobaloxime complexes that all the redox couples' reduction potentials shifted in the same direction depending on the nature of the substituent (i.e., electron-withdrawing or -donating). This is in contrast to this study, where we find that the first two reductions are minimally affected by substitution and only the last shows a significant shift.

■ CONCLUSIONS

Based on extensive computational studies and additional experiments, our main findings on the mechanism of the catalytic generation of hydrogen from water by $[(PY5Me_2)MoO]^{2+}$ are as follows:

dx.doi.org/10.1021/ja210949r | J. Am. Chem. Soc. 2012, 134, 5233−5242

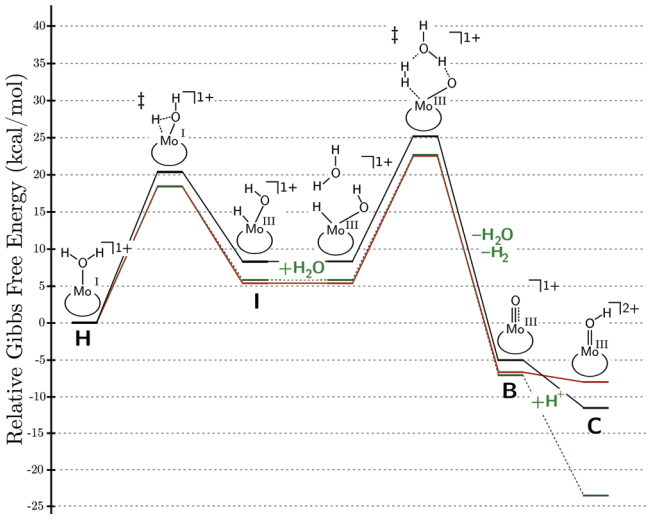

Figure 14. Gibbs free energy diagram for the liberation of hydrogen from **H**, including the two new species in Figure 13. The fluorinated species is shown the red line, and the methylated species is shown as a dotted green line; they lie almost on top of each other. The barrier for the first reaction is lowered, and that for the second remains approximately the same. Again, rather than spuriously attempt to take into account the complications involved in calculating the water association energies for a molecule already solvated in water, the complexation energy was set to 0.

(1) We have identified an experimentally and computationally consistent mechanism involving three electrochemically generated intermediates (i.e., three reductions) and two transition structures. Referring to Figure 2, our overall pathway is $\mathbf{A} \rightarrow \mathbf{C} \rightarrow \mathbf{E} \rightarrow \mathbf{H} \overset{\ddagger}{\rightarrow} \mathbf{I} + H_2O \overset{\ddagger}{\rightarrow} \mathbf{B} + H_2O + H_2 + H^+ \rightarrow \mathbf{C}$. Based on new experimental data, the first two reductions are proton-coupled.

(2) We calculated reduction potentials which are in acceptable agreement (±0.3 V) with the experimental values. The two activated steps consist of reductive cleavage of ligated H_2O, which is rate-determining, and an α-H abstraction to yield H_2 that occurs most favorably when mediated by a bridging water molecule. Calculated kinetic barriers are in reasonable agreement with the barrier inferred from the experimental turnover rate.

(3) We presented a mechanism for the stoichiometric reaction of the triflate precursor, $[(PY5Me_2)Mo(CF_3SO_3)]^+$, to yield **A** and H_2. It differs from the catalytic cycle above in that no intermediates with 1+ charge state are accessed. It is conceivable to run this mechanism under potential bias as a catalytic cycle with a lower overpotential because this cycle avoids the third reduction. However, the calculated kinetics are very slow.

(4) We have performed detailed computational analysis of the nature of the three reductions of the catalytic cycle, showing that the third reduction leads to metal orbitals that delocalize significantly onto the ligand support, in contrast to the earlier intermediates. This provides a basis for stabilizing the result of the third reduction with the use of electron-withdrawing groups. As a proof of concept, we fluorinated at the *para* positions of all the pyridine rings, which is predicted computationally to lower the potential for the final reduction by 0.2 V. The kinetics are predicted to be slightly enhanced as well.

■ ASSOCIATED CONTENT

Supporting Information

Experimental details of the CV; image displaying lability of the triflate; energetics for all functionals and species studied; further discussion of some of the LOBA results; complete ref 46; images of 3D computed structures of species not already shown in the text; Cartesian coordinates for all species studied, and X-ray crystallographic files. This material is available free of charge via the Internet at http://pubs.acs.org.

■ AUTHOR INFORMATION

Corresponding Author

mhg@cchem.berkeley.edu

Notes

The authors declare no competing financial interest.

■ ACKNOWLEDGMENTS

E.J.S. thanks the Head-Gordon group, Paul Richard Horn, and Patrick Alfonzo Shaffer for fruitful discussions. V.S.T. thanks the National Science Foundation for a graduate fellowship. This work was supported by the Director, Office of Science, Office of Basis Energy Sciences, of the U.S. Department of Energy under Contract No. DE-AC02-05CH11231.

■ REFERENCES

(1) Lewis, N. S.; Nocera, D. G. *Proc. Natl. Acad. Sci. U.S.A.* **2006**, *103*, 15729−15735.
(2) Turner, J. A. *Science* **2004**, *305*, 972−974.
(3) Cook, T. R.; Dogutan, D. K.; Reece, S. Y.; Surendranath, Y.; Teets, T. S.; Nocera, D. G. *Chem. Rev.* **2010**, *110*, 6474−6502.
(4) Sun, L.; Akermark, B.; Ott, S. *Coord. Chem. Rev.* **2005**, *249*, 1653−1663.
(5) Evans, D. J.; Pickett, C. J. *Chem. Soc. Rev.* **2003**, *32*, 268−275.
(6) Darensbourg, M. Y.; Lyon, E. J.; Zhao, X.; Georgakaki, I. P. *Proc. Natl. Acad. Sci. U.S.A.* **2003**, *100*, 3683−3688.
(7) Gloaguen, F.; Rauchfuss, T. B. *Chem. Soc. Rev.* **2009**, *38*, 100−108.
(8) Felton, G. A. N.; Vannucci, A. K.; Chen, J.; Lockett, L. T.; Okumura, N.; Petro, B. J.; Zakai, U. I.; Evans, D. H.; Glass, R. S.; Lichtenberger, D. L. *J. Am. Chem. Soc.* **2007**, *129*, 12521−12530.
(9) Du, P.; Knowles, K.; Eisenberg, R. *J. Am. Chem. Soc.* **2008**, *130*, 12576−12577.
(10) Fihri, A.; Artero, V.; Razavet, M.; Baffert, C.; Leibl, W.; Fontecave, M. *Angew. Chem., Int. Ed.* **2008**, *47*, 564−567.
(11) Baffert, C.; Artero, V.; Fontecave, M. *Inorg. Chem.* **2007**, *46*, 1817−1824.
(12) Hu, X.; Brunschwig, B. S.; Peters, J. C. *J. Am. Chem. Soc.* **2007**, *129*, 8988−8998.
(13) Wilson, A. D.; Newell, R. H.; McNevin, M. J.; Muckerman, J. T.; Rakowski DuBois, M.; DuBois, D. L. *J. Am. Chem. Soc.* **2006**, *128*, 358−366.
(14) Appel, A. M.; DuBois, D. L.; Rakowski DuBois, M. *J. Am. Chem. Soc.* **2005**, *127*, 12717−12726.
(15) Goldsmith, J. I.; Hudson, W. R.; Lowry, M. S.; Anderson, T. H.; Bernhard, S. *J. Am. Chem. Soc.* **2005**, *127*, 7502−7510.
(16) Karunadasa, H. I.; Chang, C. J.; Long, J. R. *Nature* **2010**, *464*, 1329−1333.
(17) Sun, Y.; Bigi, J. P.; Piro, N. A.; Tang, M. L.; Long, J. R.; Chang, C. J. *J. Am. Chem. Soc.* **2011**, *133*, 9212−9215.
(18) Thoi, V. S.; Karunadasa, H. I.; Long, J. R.; Chang, C. J. *Energy Environ. Sci.* **2011**, submitted.
(19) Hohenberg, P.; Kohn, W. *Phys. Rev.* **1964**, *136*, B864−B871.
(20) Kohn, W.; Becke, A. D.; Parr, R. G. *J. Phys. Chem.* **1996**, *100*, 12974−12980.
(21) Kohn, W.; Sham, L. *Phys. Rev.* **1965**, *140*, A1133−A1138.

(22) Baik, M.-H.; Friesner, R. A. *J. Phys. Chem. A* **2002**, *106*, 7407−7412.
(23) Winget, P.; Cramer, C. J.; Truhlar, D. G. *Theor. Chem. Acc.* **2004**, *112*, 217−227.
(24) Bell, A. T.; Head-Gordon, M. *Annu. Rev. Chem. Biomol. Eng.* **2011**, *2*, 453−477.
(25) Thom, A. J. W.; Sundstrom, E. J.; Head-Gordon, M. *Phys. Chem. Chem. Phys.* **2009**, *11*, 11297−11304.
(26) Li, J.; Yoshizawa, K. *Angew. Chem., Int. Ed.* **2011**, *50*, 11972−11975.
(27) Becke, A. D. *J. Chem. Phys.* **1993**, *98*, 6−10.
(28) Becke, A. D. *Phys. Rev. A* **1988**, *38*, 3098−3100.
(29) Perdew, J. *Phys. Rev. B* **1986**, *33*, 8822−8824.
(30) Chai, J.-D.; Head-Gordon, M. *J. Chem. Phys.* **2008**, *128*, 084106.
(31) Ziegler, T. *Chem. Rev.* **1991**, *91*, 651−667.
(32) Ziegler, T. *Pure Appl. Chem.* **1991**, *63*, 873−878.
(33) Szilagyi, R. K.; Frenking, G. *Organometallics* **1997**, *16*, 4807−4815.
(34) Jonas, V.; Thiel, W. *J. Chem. Phys.* **1996**, *105*, 3636.
(35) González-Blanco, O.; Branchadell, V. *J. Chem. Phys.* **1999**, *110*, 778−.
(36) Hyla-Kryspin, I.; Grimme, S. *Organometallics* **2004**, *23*, 5581−5592.
(37) Furche, F.; Perdew, J. P. *J. Chem. Phys.* **2006**, *124*, 044103.
(38) Bühl, M.; Kabrede, H. *J. Chem. Theory Comput.* **2006**, *2*, 1282−1290.
(39) Li, J. *Organometallics* **1996**, *15*, 3844−3849.
(40) Torrent, M.; Solà, M.; Frenking, G. *Chem. Rev.* **2000**, *100*, 439−494.
(41) Nemcsok, D. S.; Kovács, A.; Rayón, V. M.; Frenking, G. *Organometallics* **2002**, *21*, 5803−5809.
(42) Dolg, M.; Stoll, H.; Preuss, H.; Pitzer, R. M. *J. Phys. Chem.* **1993**, *97*, 5852−5859.
(43) Dunning, T. H. *J. Chem. Phys.* **1989**, *90*, 1007.
(44) Ahlrichs, R.; May, K. *Phys. Chem. Chem. Phys.* **2000**, *2*, 943−945.
(45) Hariharan, P. C.; Pople, J. a. *Theor. Chim. Acta* **1973**, *28*, 213−222.
(46) Shao, Y.; et al. *Phys. Chem. Chem. Phys.* **2006**, *8*, 3172−3191.
(47) Khaliullin, R. Z.; Head-Gordon, M.; Bell, A. T. *J. Chem. Phys.* **2006**, *124*, 204105.
(48) Cancès, E. *J. Chem. Phys.* **2001**, *114*, 10616.
(49) Cancès, E.; Le Bris, C. *Int. J. Quantum Chem.* **2000**, *79*, 82−90.
(50) Van Voorhis, T.; Head-Gordon, M. *Mol. Phys.* **2002**, *100*, 1713−1721.
(51) Seeger, R.; Pople, J. A. *J. Chem. Phys.* **1977**, *66*, 3045−3050.
(52) Pipek, J.; Mezey, P. *Int. J. Quantum Chem.* **1988**, *34*, 1−13.
(53) Löwdin, P. *J. Chem. Phys.* **1950**, *18*, 365.
(54) Löwdin, P. *Phys. Rev.* **1955**, *97*, 1474−1489.
(55) Miertuš, S.; Scrocco, E.; Tomasi, J. *Chem. Phys.* **1981**, *55*, 117−129.
(56) Miertuš, S.; Tomasi, J. *Chem. Phys.* **1982**, *65*, 239−245.
(57) Cramer, C.; Truhlar, D. *Chem. Rev.* **1999**, *99*, 2161−2200.
(58) Truhlar, D. G.; Cramer, C. J.; Lewis, A.; Bumpus, J. A. *J. Chem. Educ.* **2004**, *81*, 596−604.
(59) Trasatti, S. *IUPAC: Commission On Electrochemistry* **1986**, *58*, 955−966.
(60) Trasatti, S. *Electrochim. Acta* **1990**, *35*, 269−271.
(61) Donald, W. A.; Leib, R. D.; O'Brien, J. T.; Williams, E. R. *Chem.—Eur. J.* **2009**, *15*, 5926−5934.
(62) Isse, A. A.; Gennaro, A. *J. Phys. Chem. B* **2010**, *114*, 7894−7899.
(63) Tissandier, M. D.; Cowen, K. A.; Feng, W. Y.; Gundlach, E.; Cohen, M. H.; Earhart, A. D.; Coe, J. V.; Tuttle, T. R. *J. Phys. Chem. A* **1998**, *102*, 7787−7794.
(64) Coe, J. *Int. Rev. Phys. Chem.* **2001**, *20*, 33−58.
(65) Bryantsev, V. S.; Diallo, M. S.; Goddard, W. A. *J. Phys. Chem. B* **2008**, *112*, 9709−9719.
(66) Solis, B. H.; Hammes-Schiffer, S. *Inorg. Chem.* **2011**, *50*, 11252−11262.
(67) Evans, M. G.; Polanyi, M. *Trans. Faraday Soc.* **1935**, *31*, 875.
(68) Eyring, H. *J. Chem. Phys.* **1935**, *2*, 853.
(69) Goodrow, A.; Bell, A. T.; Head-Gordon, M. *J. Phys. Chem. C* **2009**, *113*, 19361−19364.
(70) Solis, B. H.; Hammes-Schiffer, S. *J. Am. Chem. Soc.* **2011**, *133*, 19036−19039.